# Effects of directly added or reaction formed TiB2 on the microstructure and mechanical properties of pressureless-sintered B4C–TiB2 composites

**Zongjia Li**
Beijing Institute of Technology
**Yangwei Wang**
Beijing Institute of Technology
**Huanwu Cheng** ( chenghuanwu@bit.edu.cn )
**Yu Zhu**
Beijing Institute of Technology
**Rui An**
Beijing Institute of Technology
**Haiyan Fang**
Beijing Institute of Technology
**Aili Feiya**
Beijing Institute of Technology
**Baofeng Han**
Beijing Institute of Technology

**Research Article**

**Keywords:** Pressureless sintering; B4C–TiB2 composites; Microstructure; Mechanical properties

**Posted Date:** March 20th, 2020

**DOI:** https://doi.org/10.21203/rs.3.rs-17972/v1

# Abstract

The boron carbide matrix composites containing boron carbide (B 4 C), titanium diboride (TiB 2 ; 20 wt% and 30 wt%) and titanium carbide (TiC) were fabricated at 2130 °C using the pressureless sintering method. Different amounts of TiB 2 and TiC particles were added to B 4 C, and the TiB 2 content was chosen as the main variable to study the effect on the composites. The density, hardness, bending strength and fracture toughness measurements were performed to obtain the physical and mechanical properties of the samples. The obtained results indicate that by adding 30 wt% TiB 2 submicron particles at 2130 °C, the bending strength and fracture toughness of 277.6 MPa and 5.38 MPa·m 1/2 are obtained for the composite. The particle pullout and crack microbridging play an effective role in toughening the composite ceramics. The main toughening mechanisms of the B 4 C-TiB 2 composites are noted to be microcrack and crack deflection toughening owing to the residual stresses resulting from the mismatch of the thermal expansion coefficient between TiB 2 and B 4 C.


# 1. Introduction

Due to its low density as well as high hardness and melting point, boron carbide ($B_4C$) is widely used for lightweight armor and cutting tools. $B_4C$ belongs to the group of non-metallic hard materials, with hardness inferior to only diamond and cubic boron nitride[1]. However, the limitations of poor toughness and sintering performance of $B_4C$ hinder its application to some extent[2–5].

Efforts have been made to enhance the sintering ability and mechanical properties of $B_4C$. Compared to the sintering methods such as hot pressing and spark plasma sintering, pressureless sintering is a relatively simple and economical method that can be used for the preparation of large and complex parts[6]. Furthermore, many additives are added to $B_4C$ to improve the ceramic properties, and the results have shown that $TiB_2$ is an ideal choice as an additive for the $B_4C$ matrix[7–10]. According to the literature studies, there are two main methods for adding $TiB_2$ in the $B_4C$ ceramics. One involves the direct addition of $TiB_2$ particles[11], whereas the other one is based on the chemical reaction of $B_4C$ with additives such as Ti[12, 13], $TiO_2$[9] and TiC[14, 15], indicating the in-situ method to prepare $TiB_2$. The addition of TiC can effectively improve the properties of $B_4C$, and the studies show that TiC reacts with $B_4C$ to form $TiB_2$ in the system (Reaction 1). However, in $B_4C$–$TiB_2$ composites field, most researches focus on reactive hot-pressing, while little researches focus on directly added or reaction formed $TiB_2$ by easy and cheap pressureless sintered. Large-scale industrial production of ceramics is hampered by the high economic and poor efficiency costs of hot-pressing.

$$2TiC + B_4C \rightarrow 2TiB_2 + 3C \qquad \text{Reaction 1}$$

Extensive studies on improving the toughness of the $B_4C$ ceramics, evolved by combining the addition of $TiB_2$ particles and pressureless sintering, are necessary. Few studies have explored the different effects of

directly added or $B_4C$-TiC reaction formed $TiB_2$ on $B_4C$ using the pressureless sintering method based on the corresponding impact on the microstructure and mechanical properties. And what remains unclear about toughening mechanism is whether two methods of forming $TiB_2$ promote each other or only one method played a major role during the synthesis. In this study, the influence of $TiB_2$ addition on the microstructure and mechanical properties of pressureless sintered $B_4C–TiB_2$ composites at 2130 ℃ has been investigated. The different addition methods were evaluated by comparing the corresponding impact on the microstructure and mechanical properties of the $B_4C–TiB_2$ composites, such as density, hardness, bending strength and fracture toughness.

## 2. Experimental Procedure

Commercially available $B_4C$ powder (~ 3.19 μm, Zhengzhou Songshan Material Co., China), TiC powder (~ 5.02 μm, Shanghai Shuitian Material Co., China) and $TiB_2$ powder (~ 0.20 μm, Shanghai Shuitian Material Co., China) were used as raw materials. Si powder (~ 2.40 μm, Shanghai Shuitian Material Co., China) and C powder (~ 0.50 μm, Shanghai Shuitian Material Co., China) were used as sintering aids, as results show that C and Si are effective sintering aids for improving the sintering ability and mechanical properties [16]. The powder mixtures of six different compositions (Table 1) were prepared by wet ball-milling at 200 rpm for 12 h in a polyethylene bottle, using $ZrO_2$ balls and alcohol medium. The weight ratio of the balls to powders was 3:1. The mixtures were dried in a rotary evaporator, followed by crushing and screening through a 100 mesh sieve. Afterwards, green compacts were formed by uniaxial pressing at about 50 MPa, followed by cold isostatic pressing at 200 MPa and sintering using a graphite element vacuum furnace at 2130 °C for 40 min. The initial heating rate was 6–8° C/min. After reaching 1800° C, the heating rate was enhanced to 9–10 °C/min. The temperature was maintained for 40 min. It was followed by cooling at a rate of 9–11 ℃/ min. After cooling down to 500 ℃, the materials were slowly cooled along with the furnace. The sintering process curve has been shown in Fig. 1.

The samples were polished and density values were measured by the standard Archimedes' method. The bending strength and the fracture toughness ($K_{IC}$) were measured on a universal testing machine (INSTRON-5985, Norwood, America). The three-point bending test with a span of 30 mm and a loading rate of 0.5 mm/min was conducted on the specimens (36.0 mm × 3.0 mm × 4.0 mm) to evaluate the bending strength; the single-edge notched beam method with a span of 30 mm and a loading rate of 0.05 mm/min was used on the specimens (36.0 mm × 3.0 mm × 6.0 mm) to measure the fracture toughness. The bending strength and the fracture toughness values were determined from the results averaged from seven bars, respectively. Crystalline phases in the sintered specimens were performed with X-Ray diffraction (XRD, Ultima III, Rigaku, Japan). Analysis of the microstructure and compositional analysis were examined by Scanning Electron Microscopy (SEM, Hitachi-S3400N, Japan).

## 3. Results And Discussion

# 3.1 Phase transition process

Figure 2 shows the XRD patterns of the as-mixed $B_4C/TiB_2/TiC/Si/C$ composite powders. As expected, $B_4C$ and $TiB_2$ are the main crystalline phases in all powder samples. Si reacted with the C powder or C element in the $B_4C$ matrix, thus, forming a SiC phase, as detected in the XRD pattern. Furthermore, it could be observed that the TiC phase disappeared, which indicated that the Reaction 1 occurred during the sintering of the ceramic samples and the TiC phase reacted completely. This suggests that the main reason affecting the microstructure and properties of the multiphase ceramics is the presence of $TiB_2$ as the second phase, for the pre-designed three-phase or two-phase ceramic systems.

# 3.2 Microstructure

The backscattered electron (BSE) images of the polished $B_4C$-$TiB_2$ composites are shown in Fig. 3. It can be seen that the $B_4C$-$TiB_2$ composites consist of three phases, the dark areas represent the $B_4C$ phase, the bright areas are the $TiB_2$ phase and the gray areas are the SiC phase. The SiC phase with small size is noted to be dispersed in the $B_4C$ matrix and presents the plate-like tissue morphology with a large aspect ratio, thus, helping to improve the mechanical properties of the whisker toughened ceramic. A small amount of laminated (white dotted bordered rectangle) and flocculated (black dotted bordered rectangle) graphite phase can also be seen in Fig. 4. Generally, there are two sources of the graphite phase. In the first case, the fine and dispersed $TiB_2$ and graphite phases were formed by the reaction of $B_4C$ with TiC during pressureless sintering, observed to be closely bound to the matrix. In the second case, the C particles used as sintering aid are graphitized at high temperature, thus, forming the graphite phase. The graphite grains promote the sintering rate as graphite located on the grain boundary inhibits the grain growth and increases the grain boundary quantity, thereby, increasing the material transport between the adjacent $B_4C$ grains, thus, promoting sintering. The graphite phase in the matrix can absorb the energy of the crack propagation by torsion, deflection and fracture under the action of the external forces. Furthermore, the crack propagation direction can be made perpendicular to the laminated graphite direction to further hinder the crack propagation.

Figure 5 and Fig. 6 show the secondary electron (SE) and BSE fracture images of the composites of Group 1 and Group 2, respectively. The porosity was observed in all samples, with Group 2 exhibiting lower porosity, thus, indicating a higher degree of densification for Group 2. It also suggested that 30 wt% $TiB_2$ could effectively improve the density of $B_4C$. The agglomerated graphite filled in the pores of the ceramic matrix is commonly observed to enhance the densification. A few sharp sintering concave necks are noted in Fig. 5a, which also confirms the reason for the low relative density of $80B_4C$-10TiC, as shown in Fig. 9a. The more rounded is the sintering neck, the fuller is the sintering, thus, the higher is the sintering density. A few regional neck growths are noted to increase and develop into a three-dimensional interpenetrating network of particles, thus, leading to further increase in the degree of densification in $70B_4C$-$20TiB_2$ and $70B_4C$-6.67TiC-$13.33TiB_2$. The pores are observed to open and get interconnected to facilitate the gas discharge in the sintering process. Thus, the microstructure of $70B_4C$-$20TiB_2$ developed more obviously, along with further densification to 98.86%. Similar phenomena is observed to occur for

Group 2 materials, as shown in Fig. 6. The sintering necks of the three samples grew, with 70$B_4C$-20TiC and 60$B_4C$-30$TiB_2$ exhibiting a higher degree of growth and fewer pores. Hence, the densification of 70$B_4C$-20TiC and 60$B_4C$-30$TiB_2$ is relatively higher in Group 2, with a relative density of 97.63% and 94.91%, respectively, as shown in Fig. 9a. It can be seen in Fig. 6d that the $TiB_2$ particles are finer and more evenly distributed than those in Fig. 6b and Fig. 6 f. The fine microstructure leads to high mechanical properties due to the Hall-Petch effect, whereas the evenly distributed particles can effectively toughen the composite ceramics, thus, resulting in optimal mechanical properties for the 60$B_4C$-30$TiB_2$ composite. Comparing the SE images with the corresponding BSE images, the fracture mode of $B_4C$ is noted to be mainly transgranular, whereas it is mainly intergranular for $TiB_2$. The mixed fracture mode is favorable for the toughness of the $B_4C$- $TiB_2$ composites, as also reported in literature [8, 9].

Figure 7 shows the crack growth path of the $B_4C$–$TiB_2$ composite. It is obvious that numerous crack deflections occurred during the crack propagation process, and the large angle crack deflection (blue dotted bordered rectangle) occurred in the two-phase junction region. Also, the crack microbridging (red dotted bordered rectangle) was observed, and the results indicated that it could improve the fracture toughness of the ceramics. Most of the cracks were observed to grow around the microcrack and pores (white dotted bordered rectangle). Besides, the grains deflected the cracks (black dotted bordered rectangle), thus, the fracture mode changed from the transgranular fracture to intergranular fracture, followed by changing back to the transgranular fracture after the crack moved around the grain. The phenomenon of crack branching can also be noted in the upper left corner of Fig. 7. As the main crack leading to the fracture expands, the evenly distributed microcracks due to the different thermal expansion coefficients of the ceramic matrix and second phase will promote the bifurcation of the main crack, thus, making the path of the main crack to become tortuous and uneven. It increases the surface energy during the expansion process, thus, hindering the rapid crack expansion and enhancing the toughness of the material, which are the fundamental reasons for the microcrack toughening. Both microcrack and crack deflection toughening result from the residual stresses caused by the mismatch in the thermal expansion coefficient of $TiB_2$ and $B_4C$. Figure 8 shows the phenomenon of the particle pullout, and a hexagonal pit 0.5 μm wide and 1 μm long can be observed. The particle pullout is a typical feature of the intergranular fracture, which can consume a large amount of crack energy, thus, improving the toughness of the composites. Overall, thhe crack deflection, particle pullout, crack microbridging, microcrack toughening and mixed fracture mode are effective means to improve the ceramic toughness. On the other hand, the thermal expansion coefficient difference between particle and ceramic matrix is the main factor determining the toughening effect.

# 3.3 Mechanical properties

The relative density, Rockwell hardness, bending strength and fracture toughness of Group 1 and Group 2 are shown in Fig. 9. It is observed that the comprehensive mechanical properties of Group 2 are better than Group 1, indicating that the composites containing 30 wt% $TiB_2$ exhibit superior mechanical performance than the composites containing 20 wt% $TiB_2$. This is attributed to an increase in the thermal

expansion coefficient of the composite with the amount of $TiB_2$. Specifically, Fig. 9a shows the relative densities of the composites. Compared to the other two components in Group 1, the maximum value is noted to be 98.86% for $70B_4C$-$20TiB_2$. It indicates that the sintering of the $B_4C$-20 wt% $TiB_2$ composite at 2130 ℃ leads to high density in the case of direct addition of the $B_4C$ powder rather than the addition of TiC or TiC and $B_4C$ mixed powders. In short, the effect of direct addition of $TiB_2$ to the composite ceramics to improve the relative density of the ceramics is observed to the most effective strategy. Similar to Group 1, the ceramic sintered with the $70B_4C$-20TiC components exhibited the highest densification in Group 2, with a value of 97.63%. Thus, in terms of the relative density of the $B_4C$-30 wt%$TiB_2$ component, direct addition of the TiC powder is more effective as compared to the addition of $B_4C$ or TiC and $B_4C$ mixed powders. In other words, $TiB_2$ generated by the in-situ reaction of TiC in the $B_4C$-30 wt%$TiB_2$ system improved the sinterability of the composite ceramics effectively. Figure 9b shows the Rockwell hardness of the Group 1 and Group 2 sintered samples. $70B_4C$-$20TiB_2$ and $60B_4C$-$30TiB_2$ exhibited the highest hardness of 85.4HRA and 86.7HRA in each group, respectively. This indicates that the $TiB_2$ particles play a key role in the hardness of the $B_4C$-$TiB_2$ composite ceramics. Moreover, compared to the reaction of TiC with $B_4C$ to form $TiB_2$, it is found that $TiB_2$, as the second phase directly added to the composites, can improve the ceramic hardness more effectively. Hence, the hardness of the composites sintered with the pre-designed $B_4C$-TiC-$TiB_2$ component is higher than the composites sintered with the $B_4C$-TiC component.

The bending strength and fracture toughness of the materials are shown in Fig. 9c and Fig. 9d, respectively. Compared with the monolithic $B_4C$ ceramics, the toughness of the $B_4C$-$TiB_2$ ceramic composites was greatly improved due to the presence of $TiB_2$. The difference in the bending strength is noted to be consistent with the change in the relative density. Generally, low densification is one of the reasons for the reduction in the bending strength, as the stress concentration tends to occur near the pores, which after a critical value leads to the material failure. The maximum bending strength among the Group 1 materials is noted for $70B_4C$-$20TiB_2$, whereas the maximum bending strength in Group 2 is observed for $70B_4C$-20TiC, with values of 308.1 MPa and 291.9 MPa, respectively. The maximum fracture toughness of the $B_4C$–$TiB_2$ composites in this study was observed to be 5.38 $MPa{\cdot}m^{1/2}$, which is more than twice the values reported for the monolithic $B_4C$ ceramics (2.4–2.6 $MPa{\cdot}m^{1/2}$)[7], rarely observed for the pressureless sintered $B_4C$ ceramics. Moreover, the fracture toughness of $70B_4C$-$20TiB_2$ and $60B_4C$-$30TiB_2$ is much higher than the other two in the group, and the material with the lowest fracture toughness among the samples has higher toughness than the monolithic $B_4C$ ceramics. It indicates that the addition of the $TiB_2$ particles can effectively improve the fracture toughness of the $B_4C$–$TiB_2$ composite ceramics, and the effect of the direct addition of $TiB_2$ particles is the most prominent. Comparing the mechanical properties of the samples, it can be observed that the two-phase system has superior properties than the three-phase system, with optimal comprehensive properties achieved by the direct addition of $TiB_2$. Also, the addition of $TiB_2$ or the incorporation of TiC to the $B_4C$ ceramics to form $TiB_2$ as the second phase represent two completely different principles. The results proved that the two

methods of forming $TiB_2$ did not promote each other and only one method played a major role during the synthesis. Moreover, the direct addition of $TiB_2$ exhibited a more important role than the use of TiC to form $TiB_2$. However, this phenomenon is dependent of the reaction conditions as the particle size, sintering temperature, sintering holding time and other conditions have an impact on the experimental results.

# 4. Conclusions

The effect of $TiB_2$ addition methods on the microstructure and mechanical properties of the pressureless sintered $B_4C$-$TiB_2$ composites at 2130 ℃ was investigated. The results indicate that the mechanical properties of the two-phase system are better than the three-phase system. Moreover, the direct addition of the $TiB_2$ powder is noted to be better than the addition of TiC or $TiB_2$ and TiC mixed powders in terms of the comprehensive mechanical properties. The $B_4C$-$TiB_2$ composites with 30 wt% $TiB_2$ added directly exhibit optimal performance, with relative density, hardness, bending strength and fracture toughness values of 94.81%, 86.71HRA, 277.6 MPa, and 5.38 $MPa{\cdot}m^{1/2}$, respectively. The toughening mechanisms are observed to be microcrack deflection, particle pullout and crack microbridging.

# References


[1] M.S. Heydari, H.R. Baharvandi，K. Dolatkhah, Effect of $TiO_2$ nanoparticles on the pressureless sintering of $B_4C$-$TiB_2$ nanocomposites. Int. J. Refract. Met. H. 51(2015) 6-13.

[2] Q. He, J. Xie, A. Wang, C. Liu, T. Tian, L. Hu, C. Yi, Z. Zhang, H. Wang, W. Wang, Z. Fu, Effects of boron content on the microstructures and mechanical properties of reactive hot-pressed BxC-TiB2-SiC composites. Ceram. Int. 45(2019) 19650-19657.

[3] F. Thévenot, Boron carbide—A comprehensive review. J. Eur. Ceram. Soc. 6(1990) 205-225.

[4] V. Domnich, S. Reynaud, R.A. Haber, M. Chhowalla, Boron Carbide: Structure, Properties, and Stability under Stress. J. Am. Ceram. Soc. 94(2011) 3605-3628.

[5] D.O. Moskovskikh, K.A. Paramonov, A.A. Nepapushev, N.F. Shkodich, A.S. Mukasyan, Bulk boron carbide nanostructured ceramics by reactive spark plasma sintering. Ceram. Int. 43(2017) 8190-8194.

[6] R.F. Speyer，H. Lee, Advances in pressureless densification of boron carbide. J. Mater. Sci. 39(2004) 6017-6021.

[7] S. Yamada, K. Hirao, Y. Yamauchi, S. Kanzaki, High strength $B_4C$–$TiB_2$ composites fabricated by reaction hot-pressing. J. Eur. Ceram. Soc. 23(2003) 1123-1130.

[8] X. Yue, S. Zhao, P. Lü, Q. Chang, H. Ru, Synthesis and properties of hot pressed $B_4C$–$TiB_2$ ceramic composite. Materials Science and Engineering: A 527(2010) 7215-7219.

[9] S.G. Huang, K. Vanmeensel, O. Van der Biest, J. Vleugels, In situ synthesis and densification of submicrometer-grained $B_4C$–$TiB_2$ composites by pulsed electric current sintering. J. Eur. Ceram. Soc. 31(2011) 637-644.

[10] Y. WANG, H. PENG, F. YE, Y. ZHOU, Effect of $TiB_2$ content on microstructure and mechanical properties of in-situ fabricated $TiB_2$/$B_4C$ composites. T. Nonferr. Metal. Soc. 21(2011) s369-s373.

[11] T.S. Srivatsan, G. Guruprasad, D. Black, R. Radhakrishnan, T.S. Sudarshan, Influence of $TiB_2$ content on microstructure and hardness of $TiB_2$–$B_4C$ composite. Powder Technol. 159(2005) 161-167.

[12] H. Cui, W. Liu, L. Cao, Q. Song, J. Tian, F. Teng, J. Wang, Effects of $B_4C$ particle size on pore structures of porous $TiB_2$–TiC by reaction synthesis. J. Eur. Ceram. Soc. 35(2015) 3381-3388.

[13] H. Wang, S. Sun, D. Wang, G. Tu, Characterization of the structure of $TiB_2$/TiC composites prepared via mechanical alloying and subsequent pressureless sintering. Powder Technol. 217(2012) 340-346.

[14] O. Popov, V. Vishnyakov, S. Chornobuk, I. Totsky, I. Plyushchay, Mechanisms of TiB2 and graphite nucleation during TiC–$B_4C$ high temperature interaction. Ceram. Int. 45(2019) 16740-16747.

[15] X. Zhang, Z. Zhang, Y. Liu, A. Wang, S. Tian, W. Wang, J. Wang, High-performance $B_4C$–$TiB_2$–SiC composites with tuneable properties fabricated by reactive hot pressing. J. Eur. Ceram. Soc. 39(2019) 2995-3002.

[16] S.S. Rehman, W. Ji, S.A. Khan, Z. Fu, F. Zhang, Microstructure and mechanical properties of $B_4C$ densified by spark plasma sintering with Si as a sintering aid. Ceram. Int. 41(2015) 1903-1906.

# Table

Table 1

Composition and nomenclature of the powder mixture.

| | Designation | $B_4C$/ wt.% | TiC/ wt.% | $TiB_2$/wt.% | C/ wt.% | Si/ wt.% |
|---|---|---|---|---|---|---|
| Sample1 | $80B_4C$-10TiC | 80 | 10 | 0 | 7 | 3 |
| | $70B_4C$-20$TiB_2$ | 70 | 0 | 20 | 7 | 3 |
| | $70B_4C$-6.67TiC-13.33$TiB_2$ | 70 | 6.67 | 13.33 | 7 | 3 |
| Sample2 | $70B_4C$-20TiC | 70 | 20 | 0 | 7 | 3 |
| | $60B_4C$-30$TiB_2$ | 60 | 0 | 30 | 7 | 3 |
| | $60B_4C$-10TiC-20$TiB_2$ | 60 | 10 | 20 | 7 | 3 |

## Figures

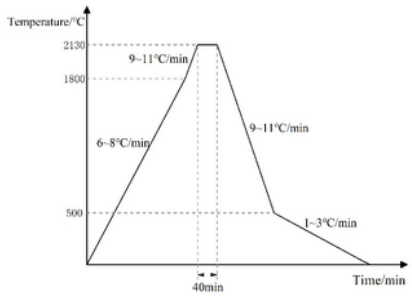


Fig. 1. The sintering process curve.

## Figure 1

The sintering process curve.

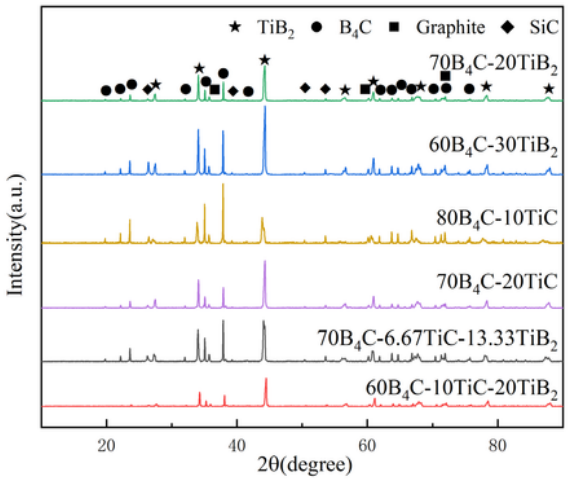


Fig. 2. XRD patterns of composites.

## Figure 2

XRD patterns of composites.

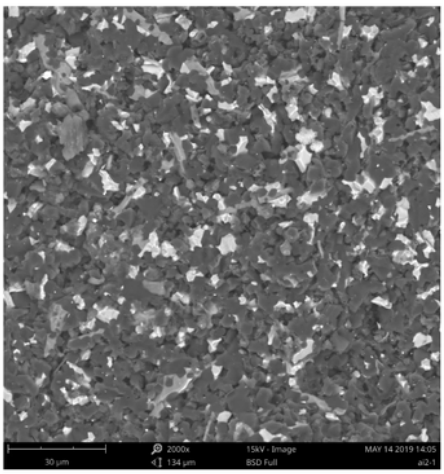


Fig. 3. BSE images of $B_4C$–$TiB_2$ composites.

## Figure 3

BSE images of B4C–TiB2 composites.

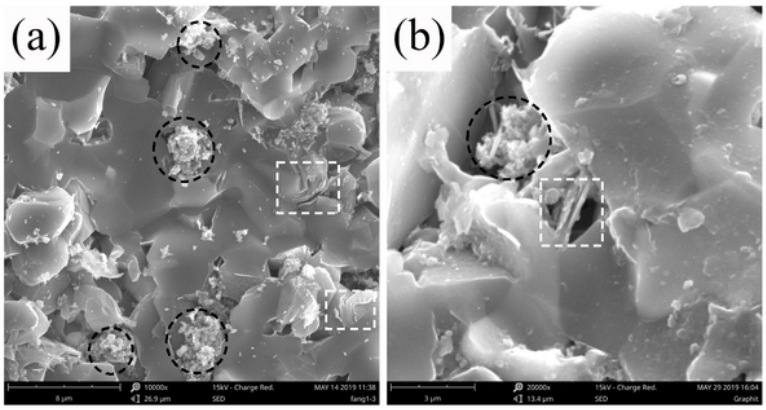


Fig. 4. SEM images of graphite phase in $B_4C$–$TiB_2$ composites: White dotted bordered rectangle is laminated graphite phase and black dotted bordered rectangle is flocculated graphite phase.

## Figure 4

SEM images of graphite phase in B4C–TiB2 composites: White dotted bordered rectangle is laminated graphite phase and black dotted bordered rectangle is flocculated graphite phase.

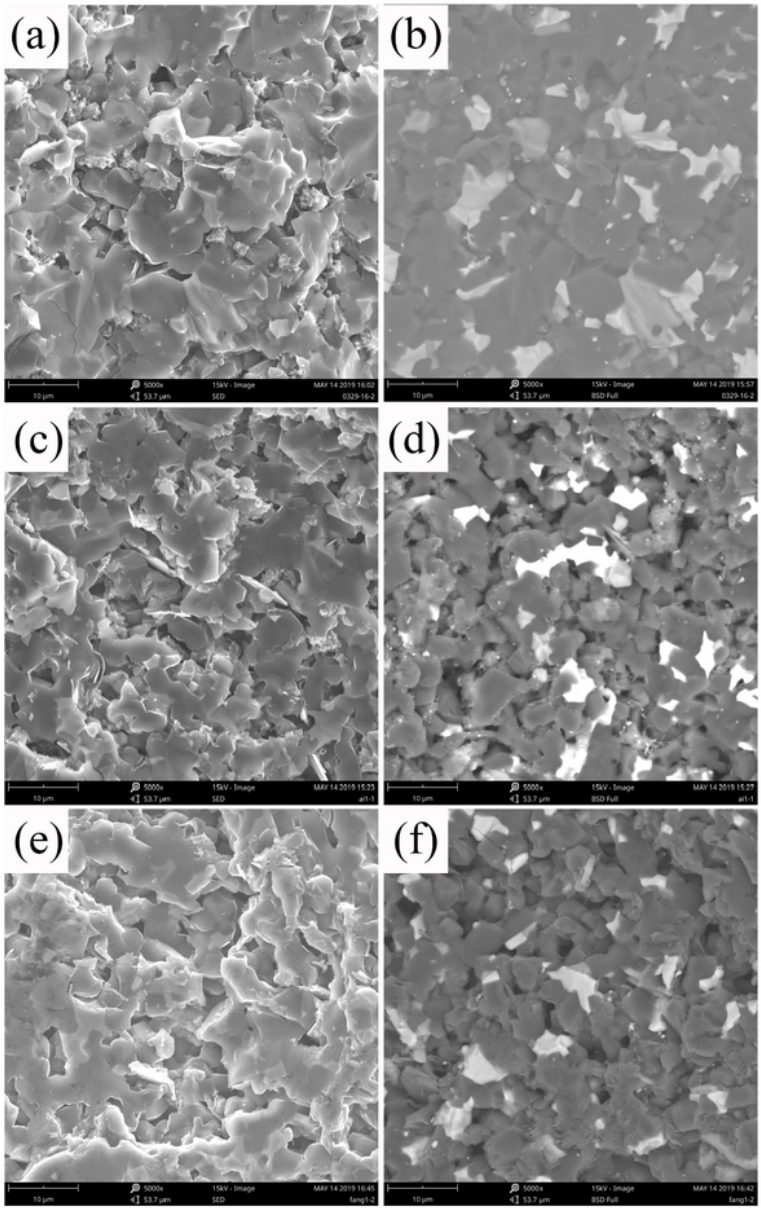


Fig. 5. SEM images of the fracture composites of Group1: (a,c,e) SE, (b,d,f) BSE; (a,b) 70$B_4C$-20$TiB_2$, (c,d) 80$B_4C$-10TiC and (e,f) 60$B_4C$-6.67TiC-13.33$TiB_2$.

## Figure 5

SEM images of the fracture composites of Group1: (a,c,e) SE, (b,d,f) BSE; (a,b) 70B4C-20TiB2, (c,d) 80B4C-10TiC and (e,f) 60B4C-6.67TiC-13.33TiB2.

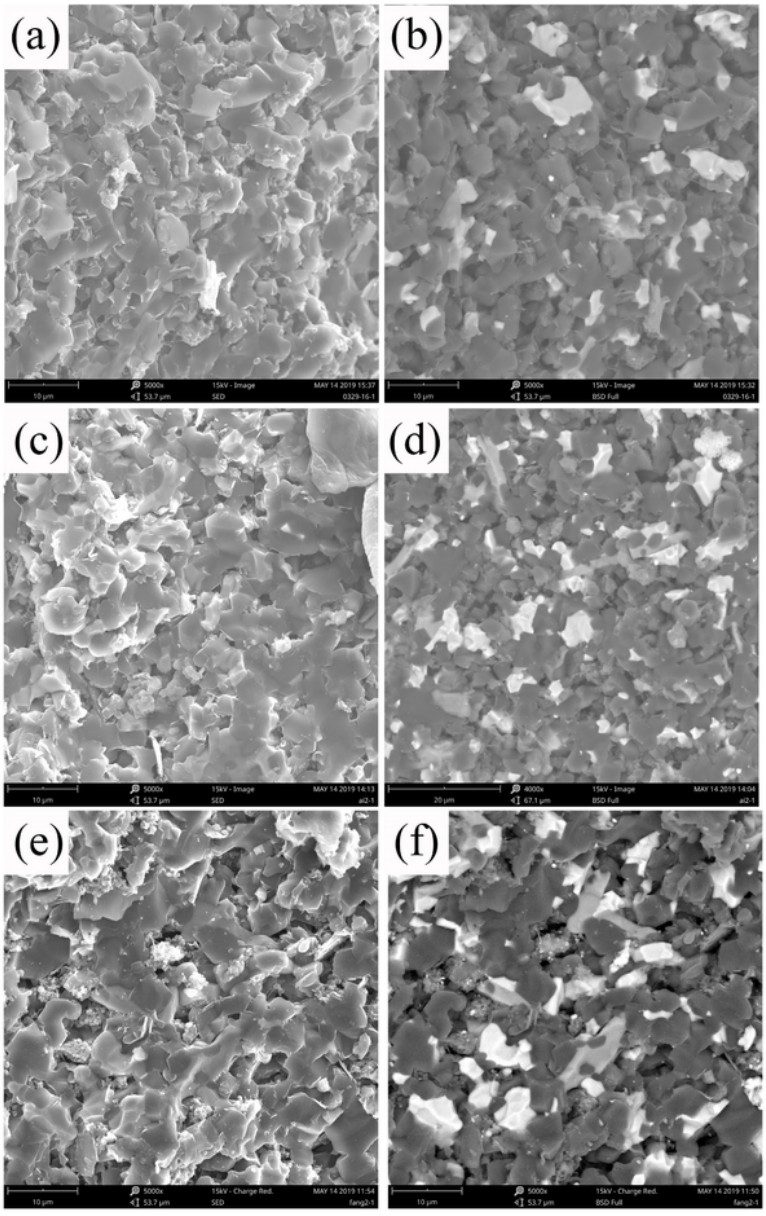


Fig. 6. SEM images of the fracture composites of Group2: (a,c,e) SE, (b,d,f) BSE; (a,b) 60$B_4C$-30$TiB_2$, (c,d) 70$B_4C$-20TiC and (e,f) 60$B_4C$-10TiC-20$TiB_2$.

## Figure 6

SEM images of the fracture composites of Group2: (a,c,e) SE, (b,d,f) BSE; (a,b) 60B4C-30TiB2, (c,d) 70B4C-20TiC and (e,f) 60B4C-10TiC-20TiB2.

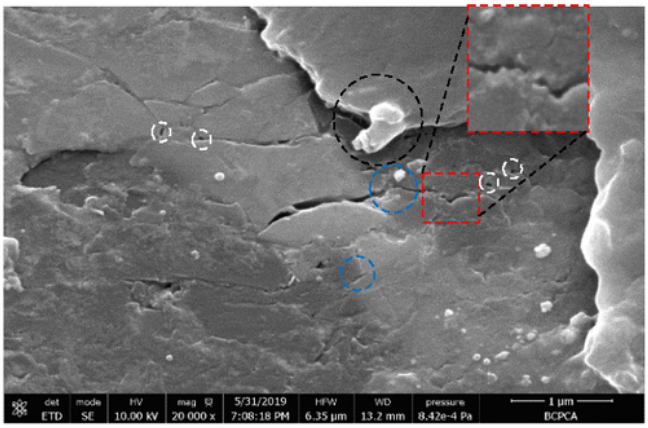

Fig.7. SEM images of the crack propagations.

## Figure 7

SEM images of the crack propagations.

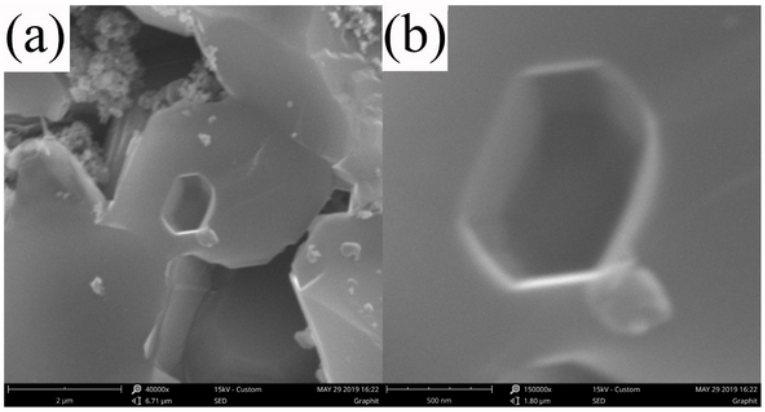


Fig. 8. SEM images of (a)the particle pullout and(b)partial enlarged view.

## Figure 8

SEM images of (a)the particle pullout and(b)partial enlarged view.

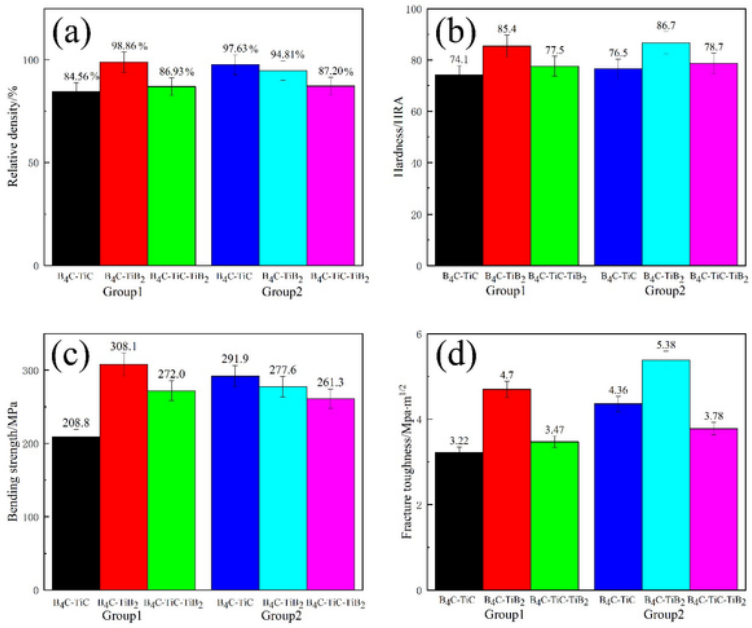


Fig.9. Mechanical properties of as-prepared $B_4C$–$TiB_2$ composites:(a) Relative density, (b) Hardness, (c) Bending strength and (d) Fracture toughness.

## Figure 9

Mechanical properties of as-prepared B4C–TiB2 composites:(a) Relative density, (b) Hardness, (c) Bending strength and (d) Fracture toughness.